




Electrochemical performance of marimocarbon/lithium titanate composites synthesized by hydrothermal method for lithium-ion batteries

Kota Hasegawa¹, Hiroyuki Gunji¹, Ryuto Kijima¹, Mika Eguchi^{1,*} , Mikka Nishitani-Gamo², Toshihiro Ando³, and Kiyoharu Nakagawa⁴

¹Institute of Quantum Beam Science, Graduate School of Science and Engineering, Ibaraki University, Hitachi 316-8511, Japan

²Department of Applied Chemistry, Faculty of Science and Engineering, Toyo University, Kawagoe 350-8585, Japan

³National Institute for Materials Science, Tsukuba 305-0044, Japan

⁴Department of Chemical, Energy and Environmental Engineering, Faculty of Environmental and Urban Engineering, and High Technology Research Core (HRC), Kansai University, Suita 564-8680, Japan

Received: 2 March 2021

Accepted: 4 July 2021

Published online:

21 July 2021

© The Author(s), under exclusive licence to Springer Science+Business Media, LLC, part of Springer Nature 2021

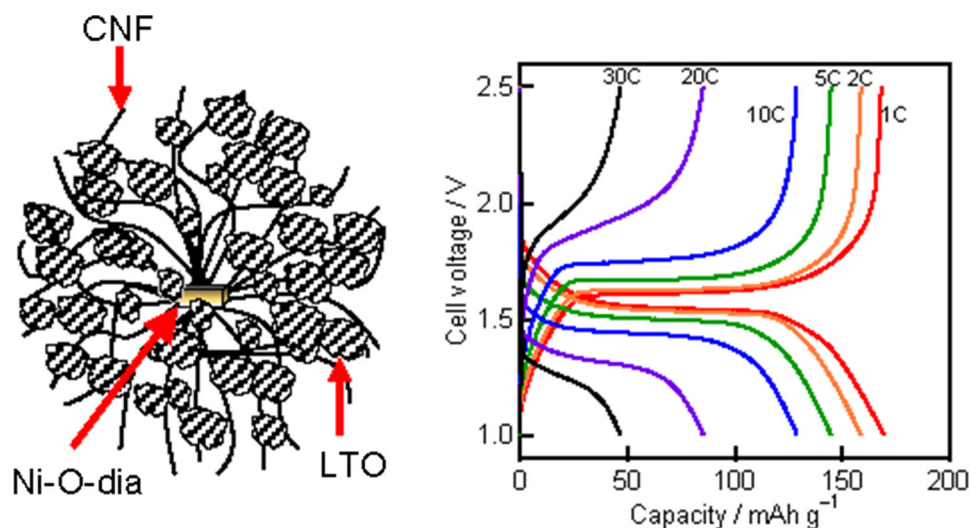
ABSTRACT

We prepared and investigated the composites of the spinel $\text{Li}_4\text{Ti}_5\text{O}_{12}$ (LTO) and Marimocarbon (MC) by the hydrothermal method that could form uniform electric paths without aggregation of the LTO particles for high capacity and high rate lithium-ion batteries. MC consisted of many fine carbon nanofilaments (CNFs) intertwined with each other in a complicated fashion. There are vacant space volumes of hundred nanometers between the CNFs. LTO particles were deposited in the space volumes among the tangled CNFs of the MCs. LTO is one of the most attractive anode materials for lithium-ion batteries because of its structural stability and safety. The morphology, microstructure and elemental composition of the LTO/MC composites were characterized by scanning electron microscopy (SEM), and X-ray diffraction (XRD). A charge–discharge test revealed that the LTO/MC composite (MC 10 wt%, prepared using a fluidized bed flow-reactor) produced the specific capacity of 170 mA g^{-1} at 1C ($1\text{C} = 175 \text{ mA g}^{-1}$). The LTO/MC composite maintained the specific capacity of 47 mAh g^{-1} even in the high rate zone at 30C whereas only the pristine LTO the produced 15 mAh g^{-1} at this rate. The unique structure of the LTO/MC composites can contribute to improving the electrochemical performance of the LTO anode. The LTO/MC composites can provide an effective approach to improve the lithium-ion battery performances.

Handling Editor: Kyle Brinkman.

Address correspondence to E-mail: mika.eguchi.m@vc.ibaraki.ac.jp

GRAPHICAL ABSTRACT



Introduction

Lithium-ion batteries are used in many electric devices, hybrid electric vehicles (HEVs) and electric vehicles (EVs) due to their high energy density, high power and long life [1–4]. The spinel $\text{Li}_4\text{Ti}_5\text{O}_{12}$ (LTO) is one of the most attractive anode materials due to its safety features. The LTO has a higher insertion potential of approximately 1.55 V versus Li^+/Li which prevents the formation of metallic lithium. The LTO also exhibits the property referred to as “zero strain” which means an excellent cycle-life during charge/discharge processes [5–10].

However, the poor electronic conductivity and lithium-ion diffusion limit its electrochemical performance [11, 12]. To enhance the performance of LTO anodes, many efforts have been reported, such as ion doping [12–14], particle size reduction [15–17], use of carbon composites [18–20].

Carbon materials are widely used as conductive additives to enhance the conductivity. Xuefei Guo et al. prepared a carbon-coated LTO using an amphiphilic carbonaceous material as a carbon precursor, and showed an excellent rate capability and cycling life [21]. Eunae Kang et al. synthesized nano-sized LTO-carbon composites by block copolymer

self-assembly and showed a highly improved electronic conductivity [22]. However, it is difficult to form a conductive path with a conventional carbon material.

Marimocarbon (MC) consists of many carbon nanofilaments (CNFs), and the CNFs are interwoven to form a spherical secondary shape. This carbon has an oxidized diamond core and radial CNFs [23, 24]. MC has a large space volume between the nanofilaments. The spaces can pass water molecules. This allows MC to easily disperse into a water solution [25] and some oxide materials can be easily deposited from ionic solutions. We have proved that MC acted as a conductive additive for anatase TiO_2 [26] and MC acted as a catalyst support for fuel cells [25, 27–30].

In this study, we synthesized LTO/MC composites by deposition of LTO particles in the spaces between the CNFs of the MC using a hydrothermal process. Figure 1 shows a schematic diagram of the LTO/MC composite in which electrolytes carry broadly. The LTO particles were dispersed in the carbon networks of the MC. There are a few aggregations of the LTO particles in the CNFs. This structure enables LTO particles to have more contact with the CNFs and electrolytes. Applying LTO/MC composites

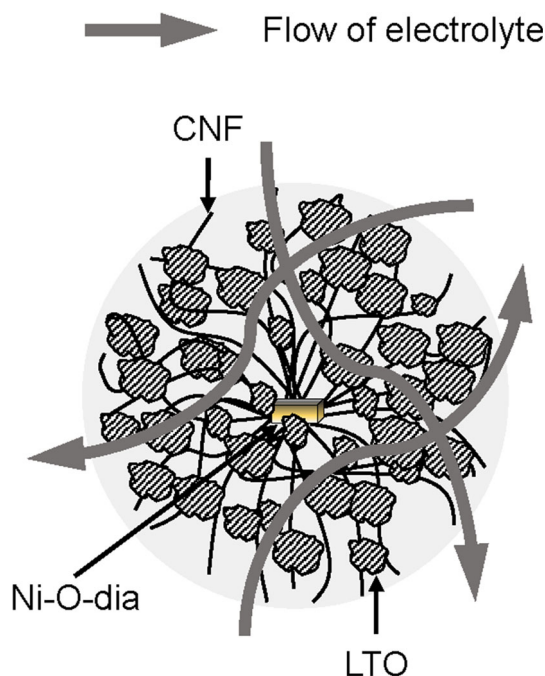


Figure 1 Schematic diagram of the LTO/MC composite.

improved the electrochemical performance of the LTO anodes.

Experimental

Preparation of LTO/MC composites

MC was synthesized by the decomposition of methane using the oxidized diamond-supported Ni catalyst [23, 24]. The reaction was carried out in a rotary or a fixed fluidized bed flow-reactor at 550 °C for 3 h (denoted MC-R or MC-F). Using MC-R prepared in a rotary fluidized bed type flow-reactor as the framework, the LTO/MC-R composites were synthesized by the deposition of Li and Ti to form LTO. Figure 2 shows the flow chart of the synthesis. Sieved MC-R smaller than 100 μm or 250 μm (MC-100R, or MC-250R, respectively) was added to 100 mL of a 0.4 M LiOH solution followed by ultrasonic wave irradiation for 1 h. The amount of the added MC-100R or MC-250R was determined to synthesize composites composed of LTO and MC in the weight ratio of 80:10 (denoted LTO/10MC-100R, or LTO/10MC-250R, respectively). The amount of LTO was based on the average amount of LTO synthesized by hydrothermal methods. Next, 5 mL of 30% hydrogen peroxide and 3.084 mL (10 mmol) of

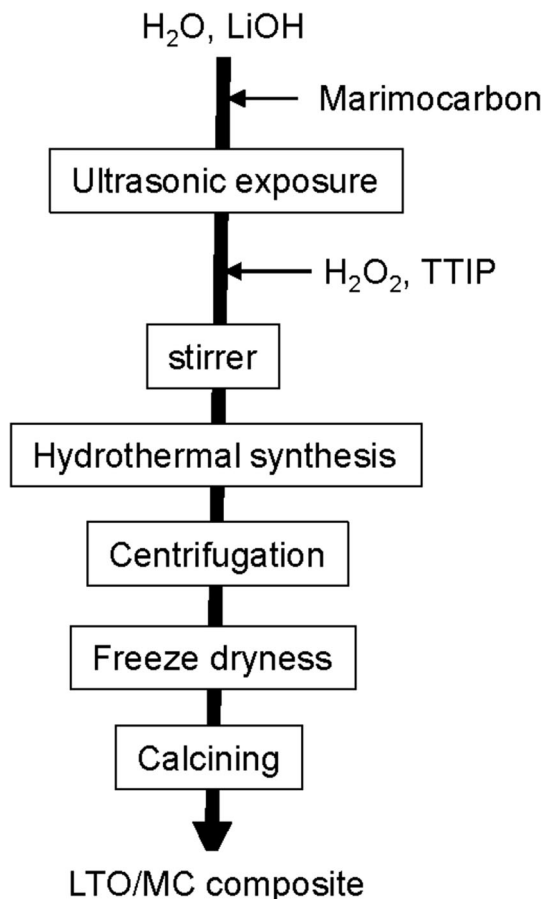


Figure 2 Flow chart of the LTO/MC composite preparation.

(C_3H_7O)₄Ti (TTIP, 97%) were added to the MC suspension. After stirring for 10 min, the obtained suspension was transferred to a Teflon-lined autoclave and placed in an oven at 130 °C for 12 h. The precipitates were washed four times with deionized water, then freeze-dried in a vacuum. Finally, the products were calcined at 400 °C for 6 h in an Ar atmosphere. Samples using MC-F prepared in a fixed bed flow-reactor were synthesized by the same process. The amount of sieved MC-F of sizes less than 100 μm or 250 μm (denoted MC-100F, or MC-250F, respectively) was determined in order to synthesize composites composed of LTO with MC-100F or MC-250F in the weight ratio of 80:10 (denoted LTO/10MC-100F, or LTO/10MC-250F, respectively). Samples using MC-100R were synthesized by the same process. The amount of added MC-100R was determined in order to synthesize composites of LTO with MC-100R in the weight ratio of 70:20 or 60:30 (denoted LTO/20MC-100R or LTO/30MC-100R). For the

blank experiment, pristine LTO without MC was prepared by the same process [31].

Characterizations

The composition and the crystalline phase of the samples were identified by X-ray diffraction (XRD, RIGAKU Ultima IV) using Cu K α radiation in the region of $2\theta = 10\text{--}80^\circ$. The surface area of the samples was evaluated by N₂ gas adsorption measurements at 77 K (SHIMADZU TriStarII 3020). The specific surface areas were calculated using the Brunauer–Emmett–Teller (BET) equation. The morphologies and microstructures of the samples were characterized by field emission scanning electron microscopy (FE-SEM, HITACHI S-4100, 15 kV).

Electrochemical measurements

The working electrodes were fabricated as follows. First, the prepared samples (LTO/MC composites, and pristine LTO) were combined with polyvinylidene fluoride (PVDF) in the weight ratio of 90:10. They were dispersed in an N-methylpyrrolidone (NMP) solvent to form homogeneous slurries. The slurry was spread on a Cu foil using an applicator and dried at 100 °C for 1 h. After drying, the Cu foil was diecut into circles (15-mm diameter), then dried under vacuum at 120 °C for 12 h. The galvanostatic charge–discharge measurements were conducted using CR2032 coin cells in an Ar-filled glove box. The coin cells were assembled using LTO/MC composites or pristine LTO as the working electrode, Li metal as the counter electrode, and a microporous polypropylene film (Celgard 2400) as the separator. The electrolyte used was 1 M lithium hexafluorophosphate (LiPF₆) dissolved in a mixture of ethylene carbonate (EC) and diethyl carbonate (DEC). The measurements were performed by a charge–discharge instrument (Hokuto Denko HJ1001SD8) at current densities between 1.0 and 2.5 V at 20 °C. Calculation of the capacities of mAh g⁻¹ is only based on the weights of LTO. Electrochemical impedance spectroscopy (EIS) measurements were conducted using a three-electrode cell in an Ar-filled glove box. Li metal was used for both the counter and reference electrodes. The same separator and electrolyte of the coin cells were used as the galvanostatic charge–discharge measurements. The tests were measured by AUTOLAB (Metrohm) in the frequency range

from 100 kHz to 0.1 Hz. The conductivities of the LTO/MC composites were evaluated by powder resistance measurements (EAGER CORPORATION).

Results and discussion

To enhance the electrochemical performances of the LTO/MC composites, we tried to reduce the particle size of the MC. Increasing the contact area for the MC can contribute to forming denser conductive paths. We succeeded in synthesizing smaller MC particles by using a rotary fluidized bed flow-reactor (Fig. 3). We synthesized more MC particles smaller than 100 μm in when using a rotary fluidized bed flow-reactor rather than a fixed bed flow-reactor. MC particles could be prevented from combining by their movement in the reactor.

Figure 4 shows the XRD spectra of the LTO/MC-100R composites containing different amounts of MC and of pristine LTO. The XRD spectra of the pristine LTO showed peaks located at 18.5°, 35.6°, 43.3°, 47.4°, 57.2°, 62.8°, 66.2°, which could be indexed as the (1 1 1), (3 1 1), (4 0 0), (3 3 1), (3 3 3), (4 4 0), (5 3 1) planes of the spinel LTO (International Center for Diffraction Data (ICDD) No. 00–049–0207), respectively. According to a prior report [32], the reaction mechanism can be proposed as follows.

The hydrolysis reaction of the TTIP aqueous solution to form TiO₂:

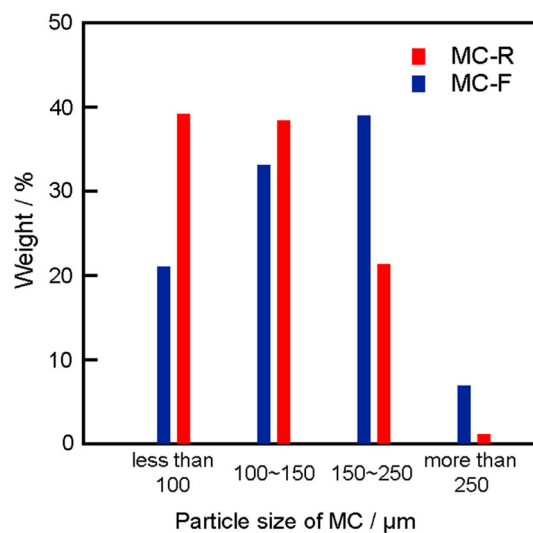


Figure 3 Particle size distribution of MC-R, MC-F.

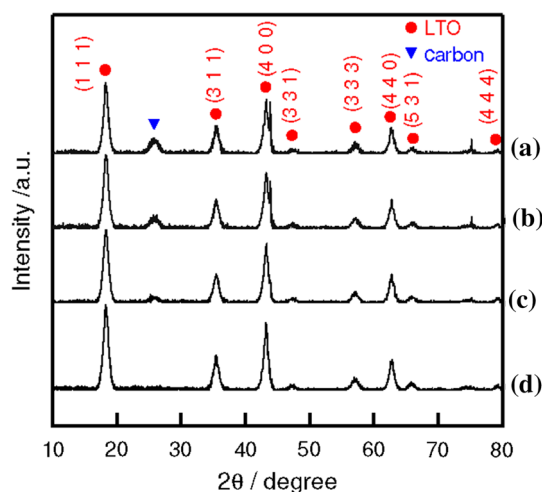
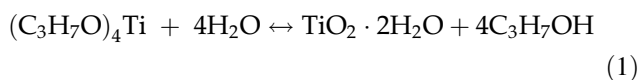
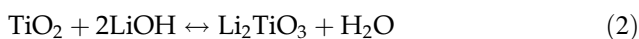


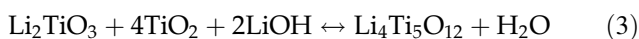
Figure 4 XRD spectra of (a) LTO/30MC-100R, (b) LTO/20MC-100R and (c) LTO/10MC-100R and (d) Pristine LTO.



Lithium-ion inserts into the TiO_2 to form mesophase lithium oxide:



Further reaction of the mesophase lithium titanium oxide and TiO_2 can form the precursor of the $\text{Li}_4\text{Ti}_5\text{O}_{12}$ phase:



In addition to these peaks, the XRD spectra of the LTO/10MC-100R composites showed a peak at 26° , which could be indexed as carbon. The XRD spectra of LTO/20MC-100R and LTO/30MC-100R showed the peaks of the spinel LTO as well as LTO/10MC-100R, along with a peak at 44° , which could be indexed as the (1 1 1) plane of diamond (ICDD No. 00-001-1249). The intensities of these peaks, which were not indexed as spinel LTO, became stronger with the increasing amount of added MC-100R. This tendency was caused by CNFs and the diamond core constructing MC-100R. Similarly, the XRD spectra of the LTO/10MC-250R, LTO/10MC-100F, and LTO/10MC-250F composites showed peaks corresponding to the spinel LTO that were derived from MC. They exhibited almost the same tendencies as the LTO/10MC-100R composites.

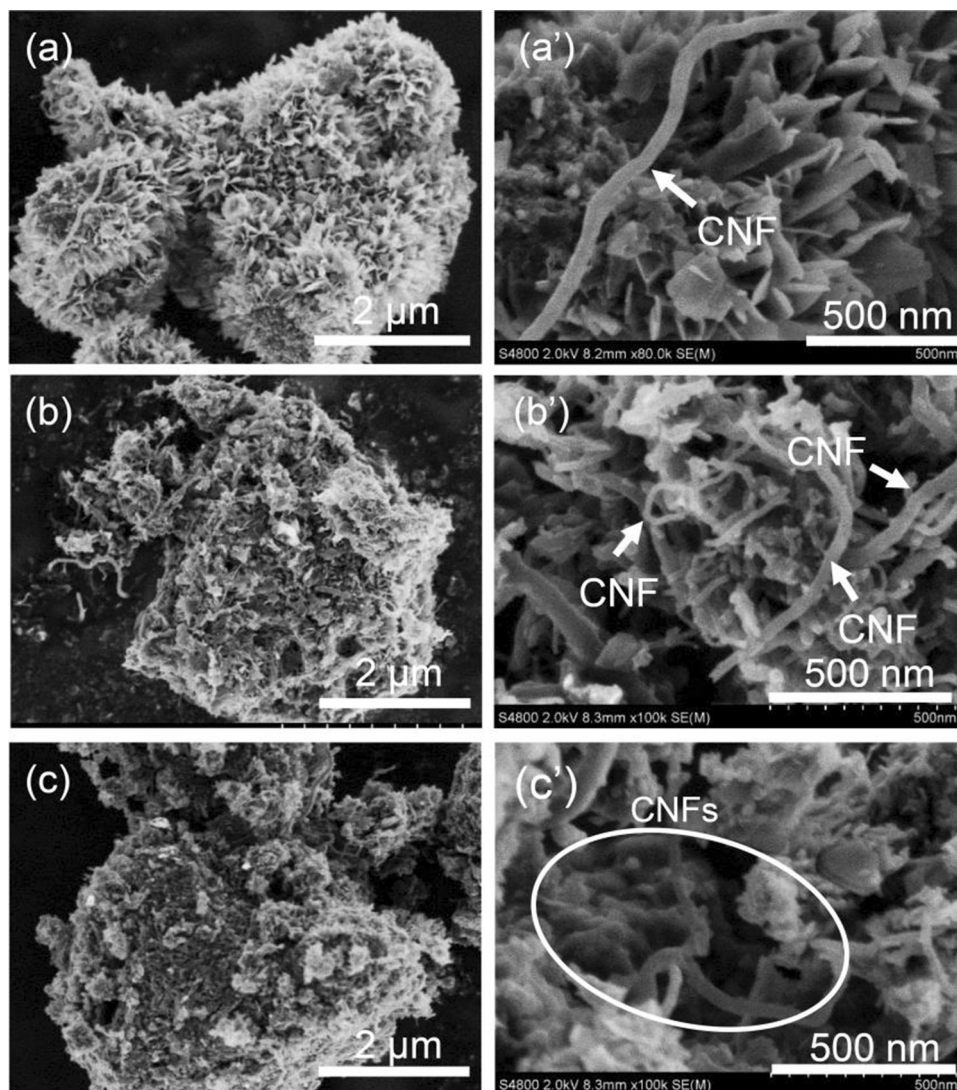
Figure 5 shows SEM images of the LTO/MC-100R composites at low and high magnifications. The low-magnification SEM images of the LTO/MC-100R

composites (Fig. 2(a)–(c)) were similar to MC. The LTO particles, which are comprised of many actuate structures, were deposited in space volume among the CNFs. This could form complex conductive networks. The high-magnification SEM images of LTO/MC-100R (Fig. 2(a')–(c')) demonstrate that more CNFs appeared with an increasing amount of added MC-100R. These suggest that the LTO particles have more contact points with the CNFs. There was no major difference among the LTO/10MC-100R, LTO/10MC-250R, LTO/10MC-100F, and LTO/10MC-250F composites in their morphologies.

The BET surface areas of LTO, MC-R, LTO/10MC-100R, LTO/20MC-100R, and LTO/30MC-100R were 120, 129, 124, 139, and $132 \text{ m}^2 \text{ g}^{-1}$, respectively. There was no major difference between the values for the MC and LTO/MC composites. This tendency was also observed in the other samples. The BET surface areas of LTO/10MC-250R, MC-F, LTO/10MC-100F, and LTO/10MC-250F were 125, 121, 119, and $125 \text{ m}^2 \text{ g}^{-1}$, respectively. These results imply that the electrolyte can easily disperse in the LTO/MC composite particles even after the LTO particles are deposited in spaces among the CNFs of MC. This can improve contact between the electrolyte and active materials, thus increasing the reaction active sites of the lithium-ion.

Figure 6 shows the charge–discharge curves of the pristine LTO and LTO/MC composites at different rates from 1 to 30 C between 1.0 and 2.5 V (vs. Li/Li^+). All the samples exhibited charge–discharge plateaus at approximately 1.55 V. Compared to the LTO/MC composites, the polarization of pristine the LTO increased more rapidly with the C-rate increasing. While the LTO/MC-R composites (Fig. 6(b), (c)) maintained nearly horizontal plateaus at 10C, the plateaus of the pristine LTO (Fig. 6(a)) sloped at the same rate. This result could indicate that the electronic conductive networks of the CNFs could effectively improve the performance of the LTO anodes. LTO/10MC-100R (Fig. 6(b)) exhibited almost the same length of its plateaus as LTO/10MC-250R (Fig. 6(c)). However, the polarization of LTO/10MC-100R was lower than that of LTO/10MC-250R in the high rate zone. This relationship between the composites using MC-R was observed in the composites prepared using MC-F. These results were attributable to increasing the contact area which formed denser electronic conductive paths. Comparing the MC-R with MC-F, the

Figure 5 SEM images of (a) (a') LTO/10MC-100R, (b) (b') LTO/20MC-100R and (c) (c') LTO/30MC-100R.



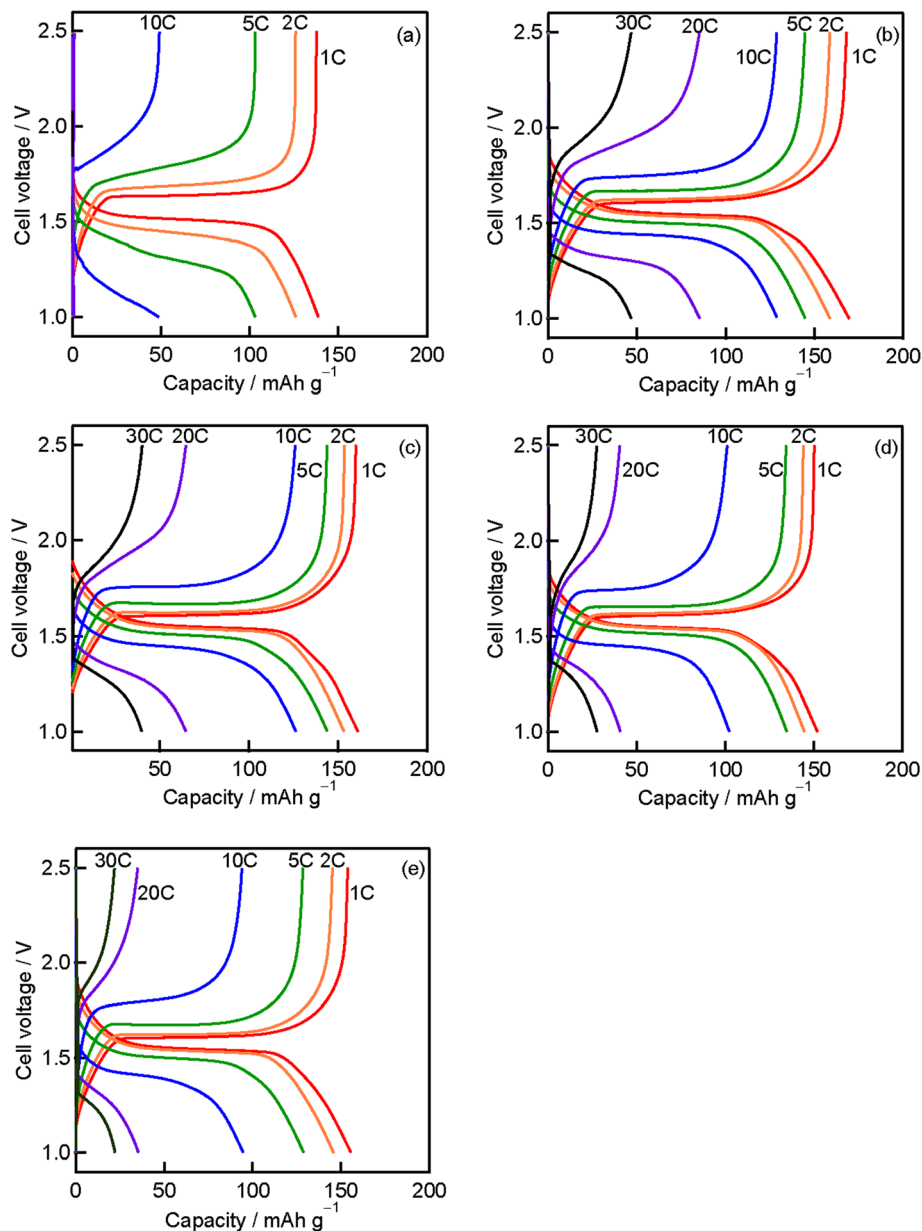
polarization of LTO/MC-100R (Fig. 6(b)) was lower than that of LTO/MC-100F (Fig. 6(d)) in the high rate zone. LTO/10MC-250R (Fig. 6(c)) and LTO/10MC-250F (Fig. 6(e)) also showed a similar relationship. MC-R contained a higher number of smaller particles than MC-F (Fig. 3), which could improve the charge-discharge performances.

Figure 7 shows comparisons of the rate performances of the pristine LTO, LTO/10MC-100R, LTO/10MC-250R, LTO/10MC-100F, and LTO/10MC-250F. The pristine LTO dramatically decreased in capacity at 10C, but the LTO/MC composites retained their capacities at the same rate. Also in the higher rate zones, the pristine LTO exhibited decreased capacities. LTO/10MC-100R and LTO/10MC-100F exhibited almost the same tendencies as LTO/10MC-250R and LTO/10MC-250F, respectively. Composites

using MC-R decreased less than the composites using MC-F, especially in the high rate zone. The discharge capacities of the LTO/10MC-100R electrode were 170, 159, 145, 129, 85, and 47 mAh g⁻¹ at 1, 2, 5, 10, 20, and 30C, respectively.

Figure 8 shows the EIS of LTO/10MC-100R and LTO/10MC-100F, while the inset is an equivalent circuit to fit the alternating current (AC) impedance spectra. R_s represents the solution resistance, R_{ct} represents the charge transfer resistance, Z_w represents the Warburg impedance, and C_d represents the double-layer capacitance. Table 1 summarizes the results of fitting the electrodes of LTO/10MC-100R, and LTO/10MC-100F. LTO/10MC-100R exhibited a lower R_{ct} (31.8 Ω) than LTO/10MC-100F (48.6 Ω). The electric conductivity of LTO/10MC-100R is higher

Figure 6 Charge–discharge curves of (a) Pristine LTO, (b) LTO/10MC-100R, (c) LTO/10MC-250R, (d) LTO/10MC-100F and (e) LTO/10MC-250F.



than that of LTO/10MC-100F. This result agreed with the charge–discharge results (Fig. 6(b), (d)).

We next investigated how the amounts of MC influenced the electrochemical performances. Figure 9 shows the powder resistances of LTO/MC-100R prepared by adding different amounts of MC-100R. The resistances decreased with the added MC-100R. This result agreed with the SEM images showing that the contact points between the LTO particles and CNFs increased with the increasing amounts of added MC. Figure 10 shows the charge–discharge curves of LTO/20MC-100R and LTO/30MC-100R. Figure 6(b) shows the charge–discharge

curves of LTO/10MC-100R as previously described. The plateaus of the LTO/MC composites in the charge–discharge curves tended to be longer at every rate with the added MC (Figs. 6(b), 10(a), (b)). This can be attributed to improvement of the electronic conductivity in the LTO/MC composites by adding more MC (Fig. 9). Figure 11 compares the rate performances of the pristine LTO, LTO/10MC-100R, LTO/20MC-100R and LTO/30MC-100R composites by adding different amounts of MC-100R. With the increasing MC-100R, the discharge capacities of the LTO/MC-100R composites increased at every rate. Although the LTO/30MC-100R composites needed

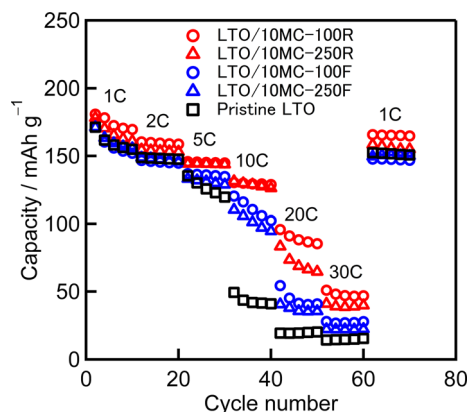


Figure 7 Rate performances of LTO/10MC with different types of added MC. Red circle: LTO/10MC-100R, Red triangle: LTO/10MC-250R, Blue circle: LTO/10MC-100F, Blue triangle: LTO/10MC-250F, Black square: Pristine LTO.

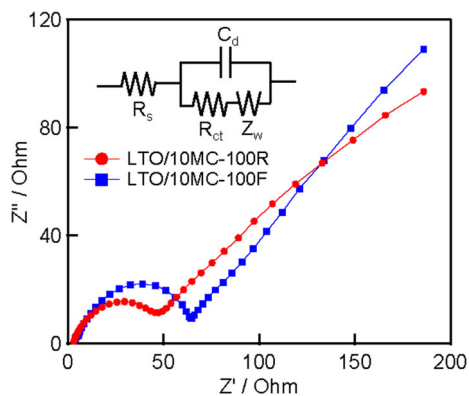


Figure 8 EIS spectra of LTO/10MC-100R and LTO/10MC-100F. The inset is the equivalent circuit model.

Table 1 Impedance parameters of LTO/10MC-100R, LTO/10MC-100F electrodes

Sample	R_s/Ω	R_{ct}/Ω
LTO/10MC-100R	3.2	31.8
LTO/10MC-100F	4.0	48.6

the highest amount of MC-100R, the LTO/30MC-100R composites showed the best electrochemical performance. The discharge capacities of LTO/30MC-100R were 183, 172, 158, 148, 134, and 113 mAh g⁻¹ at 1, 2, 5, 10, 20, and 30C, respectively.

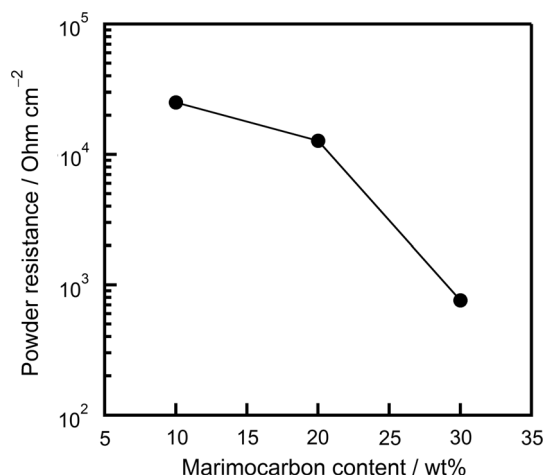


Figure 9 Powder resistances of LTO/MC-100R composites.

By adding large amounts of MC-100R, the LTO/30MC-100R composite could offer excellent electron transport. The discharge capacity could increase by adding even more MC-100R. However, some discharge capacities surpassed the theoretical capacity of the spinel LTO (175 mAh g⁻¹). Lithium-ion inserted into the graphene layers of the CNFs could have contributed to the lithium-ion storage.

Conclusions

We successfully synthesized LTO/MC composites by a hydrothermal synthesis process followed by a calcination treatment. Their uniform electric paths contributed to improving the specific capacity and rate capability compared to the pristine LTO. Sieving a smaller MC improved the charge–discharge performances. We observed that the LTO/MC composites showed increasing charge–discharge performances with the increasingly smaller MC. This is attributed to the increasing contact area. A smaller MC was synthesized by a rotary fluidized bed flow-reactor rather than a fixed type of flow-reactor. The LTO/MC composites show higher electrochemical performances when MC is synthesized by a rotary fluidized bed flow-reactor rather than a fixed type of flow-reactor. The LTO/MC composites showed higher discharge capacities with the increasing amount of added MC. This result is due to more conducting

Figure 10 Charge–discharge curves of (a) LTO/20MC-100R and (b) LTO/30MC-100R.

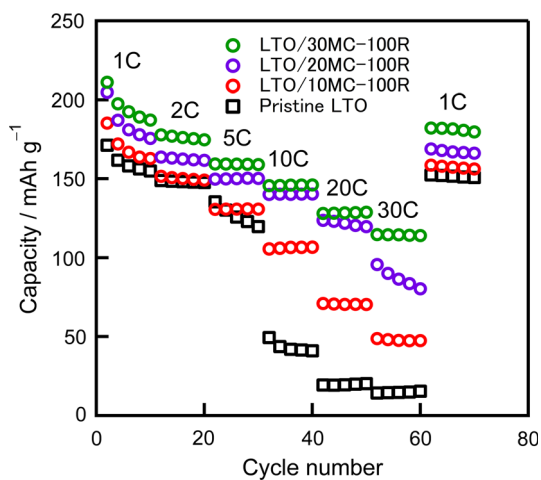
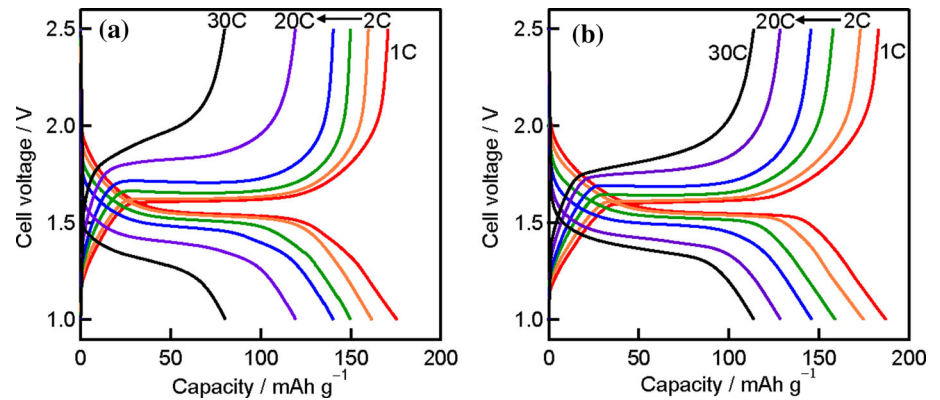


Figure 11 Rate performances of LTO/MC-100R with different amounts of added MC-100R. Green circle: LTO/30MC-100R, Purple circle: LTO/20MC-100R, Red circle: LTO/10MC-100R, Black square: Pristine LTO.

networks formed by the CNFs. In this study, the 30 wt% MC prepared using a rotary fluidized bed flow-reactor exhibited the best electrochemical performances.

We concluded that the LTO/MC composites are a promising anode material for lithium-ion batteries.

Declarations

Conflict of interest There are no conflicts to declare.

References

[1] Tarascon J-M, Armand M (2001) Issues and challenges facing rechargeable lithium batteries. *Nature* 414:359–367

- [2] Yi TF, Yang SY, Xie Y (2015) Recent advances of $\text{Li}_4\text{Ti}_5\text{O}_{12}$ as a promising next generation anode material for high power lithium-ion batteries. *J Mater Chem A* 3:5750–5777
- [3] Yang C, Kung S. j. Lin and W. C. Chien, SH (2014) $\text{Li}_3\text{V}_2(\text{PO}_4)_3/\text{C}$ composite materials synthesized using the hydrothermal method with double-carbon sources. *J Power Sources* 251:296–304
- [4] Ise K, Morimoto S, Harada Y, Takami N (2018) Large lithium storage in highly crystalline TiNb_2O_7 nanoparticles synthesized by a hydrothermal method as anodes for lithium-ion batteries. *Solid State Ionics* 320:7–15
- [5] Ferg E, Gummow RJ, Kock A, Thackeray MM (1994) Spinel Anodes for Lithium-Ion Batteries. *J Electrochem Soc* 141:L147–L150
- [6] Ohzuku T, Ueda A, Yamamoto N, Iwakoshi Y (1995) Factor affecting the capacity retention of lithium-ion cells. *J Power Sources* 54:99–102
- [7] Jansen AN, Kahaian AJ, Kepler KD, Nelson PA, Amine K, Dees DW, Vissers DR, Thackeray MM (1999) Development of a high-power lithium-ion battery. *J Power Sources* 81–82:902–905
- [8] Takami N, Inagaki H, Kishi T, Harada Y, Fujita Y, Hoshina K (2009) Electrochemical Kinetics and Safety of 2-Volt Class Li-Ion Battery System Using Lithium Titanium Oxide Anode. *J Electrochem Soc* 156:A128–A132
- [9] Goodenough JB, Kim Y (2010) Challenges for Rechargeable Li Batteries. *Chem Mater* 22:587–603
- [10] Hang T, Mukoyama D, Nara H, Takami N, Momma T, Osaka T (2013) Electrochemical impedance spectroscopy analysis for lithium-ion battery using $\text{Li}_4\text{Ti}_5\text{O}_{12}$ anode. *J Power Sources* 222:442–447
- [11] Ge H, Chen L, Yuan W, Zhang Y, Fan Q, Osgood H, Matera D, Song XM, Wu G (2015) Unique mesoporous spinel $\text{Li}_4\text{Ti}_5\text{O}_{12}$ nanosheets as anode materials for lithium-ion batteries. *J Power Sources* 297:436–441

- [12] Pu Z, Lan Q, Li Y, Liu S, Yu D, Lv XJ (2019) Preparation of W-doped hierarchical porous $\text{Li}_4\text{Ti}_5\text{O}_{12}$ /brookite nanocomposites for high rate lithium ion batteries at -20°C . *J Power Source* 437(22689):1–10
- [13] Zhang Q, Verde MG, Seo JK, Li X, Meng YS (2015) Structural and electrochemical properties of Gd-doped $\text{Li}_4\text{Ti}_5\text{O}_{12}$ as anode material with improved rate capability for lithium-ion batteries. *J Power Sources* 280:355–362
- [14] Liang Q, Cao N, Song Z, Gao X, Hou L, Guo T, Qin X (2017) Co-doped $\text{Li}_4\text{Ti}_5\text{O}_{12}$ nanosheets with enhanced rate performance for lithium-ion batteries. *Electrochim Acta* 251:407–414
- [15] Zhao S, Ka O, Xian X, Sun L, Wang J (2016) Effect of primary crystallite size on the high-rate performance of $\text{Li}_4\text{Ti}_5\text{O}_{12}$ microspheres. *Electrochim Acta* 206:17–25
- [16] Li X, Hu H, Huang S, Yu G, Gao L, Liu H, Yu Y (2013) Nano-sized $\text{Li}_4\text{Ti}_5\text{O}_{12}$ anode material with excellent performance prepared by solid state reaction: The effect of precursor size and morphology. *Electrochim Acta* 112:356–363
- [17] Kashkooli AG, Lui G, Farhad S, Lee DU, Feng K, Yu A, Chen Z (2016) Nano-particle size effect on the performance of $\text{Li}_4\text{Ti}_5\text{O}_{12}$ spinel. *Electrochim Acta* 196:33–40
- [18] Wang D, Shan Z, Liu X, Na R, Wang J, Liu H, j. Tian, (2018) High-rate $\text{Li}_4\text{Ti}_5\text{O}_{12}$ /porous activated graphene nanoplatelets composites using LiOH both as lithium source and activating agent. *Electrochim Acta* 262:9–17
- [19] H. p. Liu, G. w. Wen, S. f. Bi, C. y. Wang, J. m. Hao and P. Gao, (2016) High rate cycling performance of nanosized $\text{Li}_4\text{Ti}_5\text{O}_{12}$ /graphene composites for lithium ion batteries. *Electrochim Acta* 192:38–44
- [20] Cao N, Song Z, Liang Q, Gao X, Qin X (2017) Hierarchical $\text{Li}_4\text{Ti}_5\text{O}_{12}$ /C composite for lithium-ion batteries with enhanced rate performance. *Electrochim Acta* 235:200–209
- [21] Guo X, Wang C, Chen M, Wang J, Zheng J (2009) Carbon coating of $\text{Li}_4\text{Ti}_5\text{O}_{12}$ using amphiphilic carbonaceous material for improvement of lithium-ion battery performance. *J Power Source* 214:107–112
- [22] Kang E, Jung YS, Kim G-H, Chun J, Wiesner U, Dillon AC, Kim JK, Lee J (2011) Highly Improved Rate Capability for a Lithium-Ion Battery Nano- $\text{Li}_4\text{Ti}_5\text{O}_{12}$ Negative Electrode via Carbon-Coated Mesoporous Uniform Pores with a Simple Self-Assembly Method. *Adv Funct Mater* 21:4349–4357
- [23] Nakagawa K, Oda H, Yamashita A, Okamoto M, Sato Y, Gamo H, N-Gamo M, Ogawa K (2009) A novel spherical carbon. *J Mater Sci* 44:221–226. <https://doi.org/10.1007/s10853-008-3081-4>
- [24] Ando T, Nakagawa K, N-Gamo M, Oda H (2009) Cladophora-form carbon comprising carbon nanomaterials radially grown on a spherical core, process for producing the same and production apparatus. US Pat 7(608):331
- [25] Eguchi M, Baba K, Onuma T, Yoshida K, Iwasawa K, Kobayashi Y, Uno K, Komatsu K, KoboriN-GamoAndo MMT (2012) Influence of Ionomer/carbon ratio on the performance of a polymer electrolyte fuel cell. *Polymers* 4:1645–1656
- [26] Iwasawa K, Eguchi M, Miyoshi K, Ueda S, N-Gamo M, Ando T (2013) Preparation of TiO_2 /Marimo carbon composite. *Transactions Mater Res Soc Jpn* 38(4):573–577
- [27] Eguchi A, Okubo S, Yamamoto M, Kikuchi K, Uno Y, KobayashiN-GamoAndo MT (2010) Preparation of catalyst for a polymer electrolyte fuel cell using a novel spherical carbon support. *J Power Sources* 195:5862–5867
- [28] Eguchi M, Satou K, Iwasawa K, Nishitani-Gamo M, Ando T (2013) Preparation of the Pt-Co bimetallic catalyst on marimo carbon for PEFC. *Transactions Mater Res Soc Jpn* 38(4):549–553
- [29] Baba K, N-Gamo M, Ando T, Eguchi M (2016) Durable Marimo-like carbon support for platinum nanoparticle catalyst in polymer electrolyte fuel cell. *Electrochim Acta* 213:447–451
- [30] Baba K, N-Gamo M, Ando T, Eguchi M (2017) Preparation of catalyst for polymer electrolyte fuel cell using the Marimo-like carbon. *Transactions Mater Res Soc Jpn* 42(2):51–56
- [31] Chen J, Yang L, Fang S, Tang Y (2010) Synthesis of saw-tooth-like $\text{Li}_4\text{Ti}_5\text{O}_{12}$ nanosheets as anode materials for Li-ion batteries. *Electrochim Acta* 55:6596–6600
- [32] Wu HY, Hon MH, Kuan CY, Leu IC (2015) Hydrothermal synthesis of $\text{Li}_4\text{Ti}_5\text{O}_{12}$ nanosheets as anode materials for lithium ion batteries. *RSC Adv* 5:35224–35229

Publisher's Note Springer Nature remains neutral with regard to jurisdictional claims in published maps and institutional affiliations.